Chemical Science

ROYAL SOCIETY OF CHEMISTRY

EDGE ARTICLE

View Article Online
View Journal | View Issue

Cite this: *Chem. Sci.*, 2021, **12**, 10506

All publication charges for this article have been paid for by the Royal Society of Chemistry

A supramolecular polymeric heterojunction composed of an all-carbon conjugated polymer and fullerenes†

Shengda Wang,[a] Xingcheng Li,[a] Xinyu Zhang,[a] Pingsen Huang,[a] Pengwei Fang,[a] Junhui Wang,*[b] Shangfeng Yang,*[a] Kaifeng Wu[b] and Pingwu Du*[a]

Received 23rd June 2021
Accepted 2nd July 2021

DOI: 10.1039/d1sc03410c

rsc.li/chemical-science

Herein, we design and synthesize a novel all-carbon supramolecular polymer host (**SPh**) containing conjugated macrocycles interconnected by a linear poly(*para*-phenylene) backbone. Applying the supramolecular host and fullerene C_{60} as the guest, we successfully construct a supramolecular polymeric heterojunction (**SPh**⊃C_{60}). This carbon structure offers a means to explore the convex–concave π–π interactions between **SPh** and C_{60}. The produced **SPh** was characterized by gel permeation chromatography, mass spectrometry, FTIR, Raman spectroscopy, and other spectroscopies. The polymeric segment can be directly viewed using a scanning tunneling microscope. Femtosecond transient absorption and fluorescence up-conversion measurements revealed femtosecond (≪300 fs) electron transfer from photoexcited **SPh** to C_{60}, followed by nanosecond charge recombination to produce the C_{60} triplet excited state. The potential applications of **SPh**⊃C_{60} in electron- and hole-transport devices were also investigated, revealing that C_{60} incorporation enhances the charge transport properties of **SPh**. These results expand the scope of the synthesis and application of supramolecular polymeric heterojunctions.

Introduction

The design and fabrication of heterojunctions in varying dimensions have attracted much attention for many applications, such as transistors, solar cells, solid-state lasers, and diodes.[1–6] It is worth noting that organic heterojunctions played very important roles in organic thin-film solar cells.[7] Various organic electron-donating molecules, such as thiophenes,[8] porphyrins[9,10] and tetrathiafulvalene derivatives[11] can construct C_{60}-based donor–acceptor (D–A) heterojunction systems, which can effectively suppress aggregation of fullerene derivatives and facilitate energy conversion. Imahori and co-workers reported porphyrin/C_{60} composite clusters and discovered photocurrent generation under light irradiation.[12,13] Inspired by these studies, crown-shaped small molecular heterojunctions were constructed using curved nanographene host molecules for photocurrent generation.[14] Supramolecular polymers are regarded as an important source of intelligent materials and show broad applications.[15–19] These supramolecular structures can be formed by various different interactions, such as metal coordination,[20,21] π–π stacking,[22] host–guest recognition,[23–25] and hydrogen bonding.[26,27] Würthner and co-workers achieved a co-assembled p–n-junction on a nanoscopic scale containing a p-type oligo(*p*-phenylene vinylene) donor and an n-type perylene bisimide acceptor, which are initially formed *via* hydrogen bonding and subsequently self-assemble into chiral stacks by π–π interactions.[28] Aida and co-workers reported an unusual supramolecular polymerization reaction upon heating as well as cooling using a metalloporphyrin-based tailored monomer to investigate its stimuli-responsive applications.[29] Recently, frustrated Lewis pairs were implemented into supramolecular polymers combined with π-conjugated O-bridged triphenylborane and triphenylamines by Meijer and co-workers.[30] The Yang group reported novel supramolecular polymeric nanoparticles comprised of chromophoric guest molecules and disulfidebridged bispillar[5]arene to construct a light-harvesting system.[31] However, the construction of highly ordered, multi-stage, multilayered polymeric supramolecular systems is still an unsolved challenge.[32,33] The structural effects of charge mobilities in supramolecular polymeric heterojunction systems have been rarely explored.

Conjugated polymers (CPs) have attracted great interest for various optoelectronic applications due to their

[a]*Hefei National Laboratory of Physical Science at the Microscale, CAS Key Laboratory of Materials for Energy Conversion, Department of Materials Science and Engineering, iChEM (Collaborative Innovation Center of Chemistry for Energy Materials), University of Science and Technology of China (USTC), 96 Jinzhai Road, Hefei, Anhui Province, 230026, P. R. China. E-mail: dupingwu@ustc.edu.cn; sfyang@ustc.edu.cn; Fax: +86-551-63606207*

[b]*State Key Laboratory of Molecular Reaction Dynamics, Dynamics Research Center for Energy and Environmental Materials, Dalian Institute of Chemical Physics, Chinese Academy of Sciences, Dalian, Liaoning 116023, P. R. China. E-mail: wjh@dicp.ac.cn*

† Electronic supplementary information (ESI) available. See DOI: 10.1039/d1sc03410c

semiconductivity in pristine (neutral) or doped states.[34] CPs generally exhibit an efficient absorption or emission at the band edge.[35] For example, excitons with bounded electron–hole pairs are created to emit strong luminescence when photons are absorbed in poly(phenylenevinylene) materials.[36] The wide band-gap poly(*p*-phenylene) (PPP) materials have a rigid-rod character and contain very stable benzene rings.[37] Therefore, much attention has also been paid to their synthesis and electronic properties.[38–43] Linear or cyclic benzene rings in PPP and cyclo-*para*-phenylene (CPP) macrocycles can be considered as conjugated segments of graphene nanoribbons and single-walled carbon nanotubes (SWCNTs).[44–49] In addition, it has been found that these macrocycles show good supramolecular interactions with fullerenes such as C_{60} (ref. 50 and 51) and C_{70}.[52] Their electron transfer properties between a macrocycle and fullerenes have been recently investigated by von Delius and Guldi,[53,54] Martín,[55] and our group.[52,56,57] Thus, integrating the physical properties of macrocycle-based conjugated polymers and fullerenes to make supramolecular polymeric heterojunctions could have many interesting properties and applications in molecular electronics and materials.[58]

Herein, we report design and synthesis of a novel PPP-based supramolecular polymeric heterojunction containing conjugated macrocycles interconnected by a PPP backbone, which acts as a supramolecular host to form a host–guest supramolecular polymeric heterojunction with fullerene C_{60} (**SPh**$\supset C_{60}$), representing the first polymeric segment of the supramolecular heterojunction of carbon nanopeapods (Fig. 1). In specific, the conjugated macrocycles mimic the curved polyphenylene-C_{60} peapod segment of a CNT, and the linear PPP backbone is the linear polyphenylene part along the CNT. This polymer was fully characterized by different techniques. In addition, the supramolecular interactions between **SPh** and fullerene C_{60} were investigated. Moreover, transient absorption measurements were performed to investigate the charge transport dynamics between **SPh** (electron donor) and C_{60} (electron acceptor). The charge transport properties of the supramolecular polymeric heterojunction were examined using the space charge limited current (SCLC) method, revealing that C_{60} incorporation enhances the charge transport properties of **SPh**.

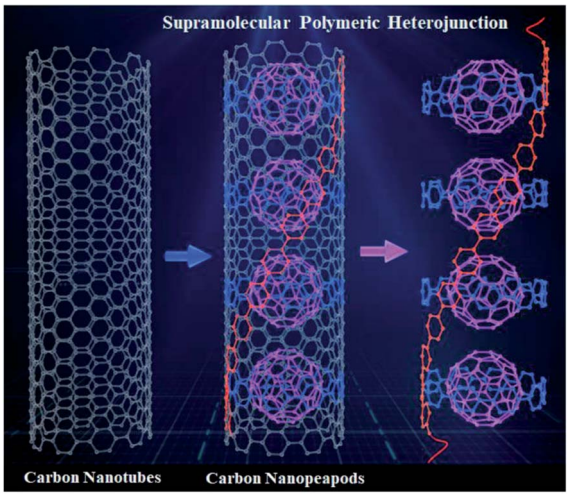

Fig. 1 The design of a novel conjugated polymer (SPh) containing a conjugated macrocyclic host and a poly(*para*-phenylene) (PPP) backbone, representing the first supramolecular polymeric heterojunction as the segment of carbon nanopeapods.

Results and discussion

Molecular design of SPh

To obtain the target supramolecular polymeric heterojunction as the segment of carbon nanopeapods with desired structural features, the appropriate functional building unit for π-extension should be rationally selected. Thus, a bifunctional conjugated macrocyclic host with the reaction sites in the *para* position will be a good candidate for both linear polymeric π-extension and supramolecular interaction. A previous study showed that a cyclic precursor can react with the linear component containing three phenyl rings.[56] Then, a tetra-substituted phenylene unit with different reaction sites can connect with the cyclic molecule by the Suzuki–Miyaura coupling reaction to achieve the bifunctional monomer and subsequently to form a long π-conjugated PPP-based polymeric segment of CNTs. Once fullerene molecules are embedded into CPP moieties of the conjugated polymer, a polymeric segment of carbon nanopeapods can be achieved.

Synthesis of SPh

The synthesis procedure for **SPh** is summarized in Fig. 2. Compound 2′,5′-dibromo-4,4″-dichloro-1,1′:4′,1″-terphenyl (**1**) was prepared according to our previously reported procedure.[56] Then, two bromo groups in **1** were transformed into 4,4,5,5-tetramethyl-1,3,2-dioxaborolane groups by Pd-catalyzed borylation to produce compound **2** in a yield of ∼60%. Subsequently, linear compound **2** was embedded into the ring-shaped structure to generate the monomer for polymerization. Under the standard conditions for a Pd-catalyzed Suzuki coupling reaction, compound **2** reacted with the curved precursor 3 to synthesize the key macrocycle intermediate **4**, which was successfully converted into the targeted macrocyclic monomer **5**, a light yellow solid, by an aromatization reaction. All these small molecules were fully characterized by NMR, and MS (Fig. S16–S23†). Finally, a polymerization reaction using compound **5** was carried out in dry DMF by a nickel-mediated Yamamoto homocoupling reaction, and the polymer **SPh** was then obtained as an intense yellow solid in a yield of ∼72%.

Characterization of the SPh and SPh$\supset C_{60}$

The successful synthesis of π-extended polymer **SPh** from compound **5** was confirmed by gel permeation chromatography (GPC), FTIR, mass spectrometry, and Raman spectroscopy. After the polymerization reaction, Soxhlet extractions with methanol and acetone were performed to remove lower molecular weight oligomers; the GPC molecular weight data for **SPh** are presented in Fig. 3a and S1.† The weight average molecular weight (M_w), relative number-average molecular weight (M_n), and polydispersity index (PDI) of **SPh** were measured, and the results

showed that M_n = 10 768 g mol^{-1} using polystyrene as the standard. This weight is approximately equal to 11 repeating units. The large PDI value at 2.66 suggested a broad molecular weight distribution. The mass spectra are shown in Fig. S2 and S7,† demonstrating different lengths of the polymeric molecules with roughly similar mass distribution results before and after the chromatographic purification of the polymer. This is probably due to the high molecular weight, low solubility, and some aggregation in **SPh**, which make purification of each oligomer very difficult. MALDI-TOF MS spectrometry data of **SPh** show a series of equidistant mass peaks in the high-molecular-weight fraction with up to 17 repeating units. The m/z and interval values ($\Delta m/z$ = 910.36) are consistent with the calculated values, indicating the successful polymerization of compound **5**.

Moreover, we compared the GPC traces of **SPh**⊃C_{60} in different solvents (Fig. S10†). Only small oligomers are present, probably due to the poor solubility of **SPh**⊃C_{60} in chloroform ($CHCl_3$) and *N*,*N*-dimethylformamide (DMF) (Fig. S10c†). It should be noted that the concentration for GPC was approximately 5 mg mL^{-1} and substantial insolubilities in the concentrated solutions cannot be introduced into the mobile phase. Thus, the results only reflect smaller soluble oligomers dissolved in $CHCl_3$ and DMF. In addition, **SPh**⊃C_{60} was further characterized by FTIR (Fig. S8†). C_{60} contains the C–C bond and C=C bond, and four absorption peaks are found in the FTIR spectra of **SPh**⊃C_{60} at 526, 576, 1161, and 1430 cm^{-1}, respectively. Compared with the FTIR spectrum of **SPh**, the results suggest the formation of a supramolecular polymeric heterojunction (**SPh**⊃C_{60}). Raman spectroscopy was also used to characterize **SPh**⊃C_{60}. In Fig. S9,† the Raman dominant peak of **SPh**⊃C_{60} at 1469 cm^{-1}, indicating the stretching mode of cages of C_{60}, slightly shifted compared with that of C_{60} (1468 cm^{-1}), which is similar to C_{60}-β-CDP reported by Diao and co-workers.[59,60] These results indicate that the formation of supramolecular complexes (**SPh**⊃C_{60}) did not change the nature of C_{60}. No appreciable Raman peaks of **SPh** can be recognized in **SPh**⊃C_{60}, probably due to the strong fluorescence background signal of **SPh**.

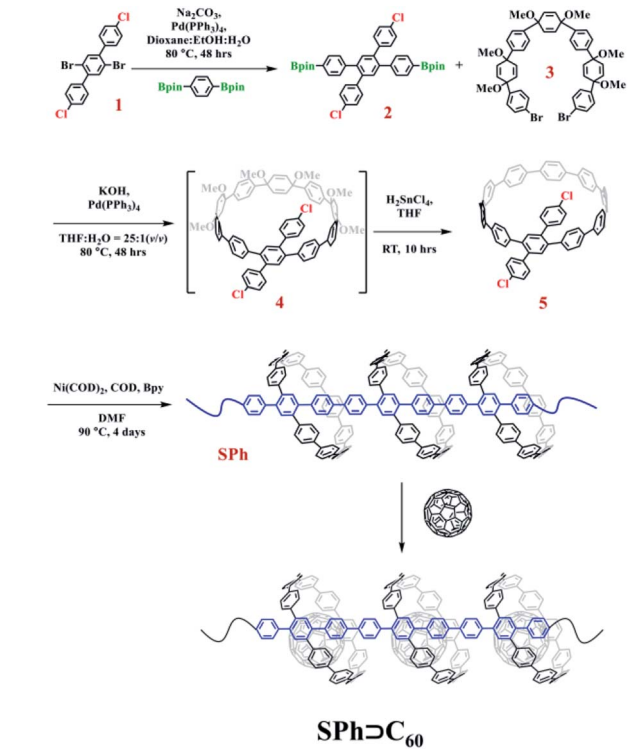

Fig. 2 Synthesis procedure for compound **5** and the polymeric segment of carbon nanopeapods (**SPh** and **SPh**⊃C_{60}).

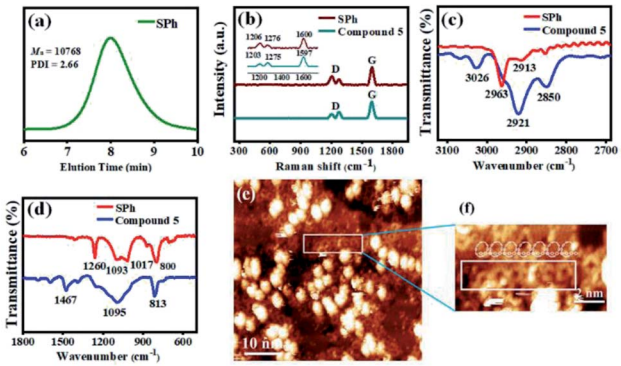

Fig. 3 (a) GPC trace of **SPh**. (b) Raman spectra (excited at 785 nm) of **SPh** (wine) and **5** (dark cyan). (c and d) FTIR spectra of **SPh** (red) and compound **5** (blue). (e) A high resolution STM image showing the polymer segment **SPh**. The sample was prepared by the simple drop casting method. Imaging conditions: U = 1.3 V, I = 20 pA. (f) A smaller area STM image showing the existing morphology of the target polymer segment with the hoop-shaped structure.

Raman spectroscopy was further used to characterize **SPh**. Fig. 3b, S3, and S4† show the Raman spectra of **SPh** and monomer **5**. A strong Raman G-band appears at approximately 1600 cm^{-1} for both **SPh** and compound **5**, which probably arises from the symmetrical vibration caused by the collective C–C stretching modes of the benzenoid rings along the transverse tube axis. The D-band at ~1200 cm^{-1} mainly originates from the in-plane C–H bending modes, and those around 1270 cm^{-1} correspond to ring breathing modes. In addition, the main peaks of [10]cyclo-*para*-phenylene were at 1206, 1265, and 1582 cm^{-1},[61] and the signals of linear PPP are located at 1215, 1285, and 1602 cm^{-1}.[62] Some of these peaks are quite similar to signals of **SPh**, which further confirms the existence of cyclo-*para*-phenylene macrocycle and one-dimensional PPP structures. All these results suggest the polymerization of monomer 5 and the formation of **SPh**.

The FTIR spectra also demonstrate the successful polymerization of compound **5** into **SPh** (Fig. 3c, d, S5 and S6†). Fig. 3c shows the C–H stretching of **5** and **SPh** in the high wavenumber region. Three obvious peaks (3026 cm^{-1}, 2921 cm^{-1}, and 2850 cm^{-1}) were observed for compound **5**. In sharp contrast, only the peak located at 2913 cm^{-1} appears for **SPh**. In the FTIR spectra of the low wavenumber region (Fig. 3d), significant differences were also observed for **SPh** (mainly four peaks at 1260 cm^{-1}, 1093 cm^{-1}, 1017 cm^{-1}, and 800 cm^{-1}) and

compound **5** (two sharp peaks at 1467 cm^{-1} and 813 cm^{-1}, and one broad band maximized at 1095 cm^{-1}). Similar peaks at 813 cm^{-1} for **5** and 800 cm^{-1} for **SPh** are associated with out-of-plane C–H deformation from the vibration of a *para*-disubstituted benzene ring. Moreover, the peak at 1467 cm^{-1} for compound **5** is completely gone after polymerization. A new peak at ~1260 cm^{-1} appears in **SPh**, consistent with the FTIR spectrum of PPP polymers.[62]

The polymeric chains of **SPh** composed of a conjugated hoop-shaped structure were further confirmed by the scanning tunneling microscope (STM) imaging technique at the submolecular level. Using a drop casting method, the high-resolution STM image with a singly dispersed carbon nanohoop structure is shown in Fig. 3e. Many hoop-shaped structures with a disordered arrangement were adsorbed onto the surface, as well as a lot of aggregated particles with bright spots. To clearly observe the morphology of the polymeric segment, an enlarged image is shown in Fig. 3f. To test the composition of these tiny spots, an energy-dispersive X-ray spectroscopy (EDX) experiment was conducted and the results showed that these tiny spots should be carbon-containing moieties (see Fig. S11†). The polymeric chain containing around seven conjugated macrocycles can be identified and the hoop-shaped structure was clearly recognized, confirming the contracture of **SPh**.

Photophysical properties of SPh

The photophysical properties of **SPh** and monomer **5** were investigated in solution by UV-vis absorption spectroscopy, steady-state fluorescence spectroscopy, and time-resolved fluorescence decay spectroscopy (Fig. 4). The absorption spectrum of **SPh** showed an intense absorption band maximized at ~326 nm with a shoulder band in the range of 372–432 nm, which is slightly redshifted compared to **5** (maximized at ~317 nm). Because of the same CPP skeletons, **SPh** and **5** show nearly the same fluorescence spectra with maximum peaks at ~470 nm and 465 nm, respectively. The fluorescence quantum yields determined for compound **5** and **SPh** are $\Phi_F = 23\%$ for **SPh** and $\Phi_F = 14\%$ for **5** (using anthracene in ethanol as reference, $\Phi_F = 30\%$). Both values are much lower than that of [10]CPP ($\Phi_F = 65\%$),[63] probably because the functionalized benzene rings increase the proportion of nonradiative decay of the excited states. The fluorescence colors of **SPh** and **5** are shown in Fig. 2b, indicating their similarity on emitting blue fluorescence.

The luminescence lifetimes (τ_s) of **SPh** and **5** were further measured by the time-resolved photoluminescence (TRPL) technique using a nanosecond pulsed laser system (Fig. 4c and d). The fluorescence decay of **5** follows first-order kinetics with a lifetime $\tau_s = 2.7$ ns at 469 nm when excited at ~300 nm. **SPh** shows a similar single-exponential decay with a much longer fluorescence lifetime of $\tau_s = 18.7$ ns. Based on the above results, the similarity of these optical properties for **SPh** and **5** in solution indicates that the motif of cyclo-*para*-phenylene plays an important role.

Supramolecular chemistry and ultrafast excited-state dynamics

For a long time, fullerenes have been widely studied as guests in various organic host architectures owing to their unusual shape (approximately spherical) and chemical nature (nonpolar polyenes).[55] These organic host architectures have specific sizes for C_{60} to construct various host–guest molecular systems *via* supramolecular interactions and weak supramolecular van der Waals interactions, such as supramolecular organic frameworks,[64] cyclodextrin,[65] calix[8]arene,[66] crown ether,[67,68] macrocyclic bis-exTTF hosts,[50] and nanorings.[51,69] Cyclo-*para*-phenylene with ten phenyl groups has an appropriate size to complex with C_{60}, as evidenced by single crystal X-ray diffraction analysis and NMR studies.[69,70] These results confirmed that such a conjugated macrocycle has the right size to selectively encapsulate C_{60}. Recently, π-extended crown-shaped CPPs[56] and porphyrin-embedded nanorings[71] showed highly enhanced binding constants with fullerenes C_{60}. Their supramolecular structures with C_{60} can also be directly observed by single-crystal X-ray diffraction. All these results make it possible for **SPh** to form a host–guest supramolecular polymeric heterojunction with fullerene C_{60} (**SPh**⊃C_{60}).

Based on its structure, **SPh** contains a macrocyclic unit for C_{60} to construct the designed carbon nanopeapod segment. We performed UV-vis experiments and fluorescence quenching experiments on the C_{60} titration to confirm the existence of the supramolecular interactions between **SPh** and C_{60}. When C_{60} was added into a **SPh** solution in toluene, the solution color obviously changed from yellow to brown. Upon C_{60} titration into the **SPh** solution, the absorption spectra of **SPh** showed an obvious enhancement in the range of 280–430 nm (Fig. 5a). The absorption band maximum at ~330 nm should be mainly due to the presence of C_{60}. Also, the fluorescence intensity was significantly reduced under a hand-held UV lamp excited at

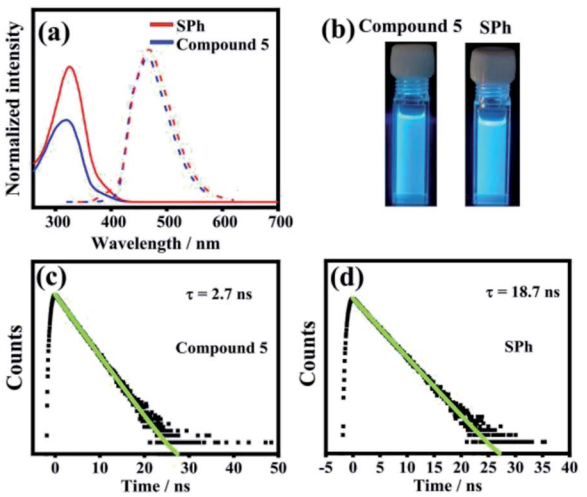

Fig. 4 (a) UV-vis absorption (solid line) and fluorescence (dot line) spectra of **SPh** (red) and compound **5** (blue) in CH_2Cl_2. (b) **SPh** and compound **5** in CH_2Cl_2 solution under UV irradiation at 365 nm. Emission lifetimes for compound **5** (c) and **SPh** (d) in CH_2Cl_2.

365 nm; measurements of its emission intensity during titration (Fig. 5b) suggest that fullerene C_{60} can efficiently quench the fluorescence. Monomer **5** was chosen to study the supramolecular interaction with C_{60} by fluorescence spectroscopy. The titrating results showed that its K_a is $\sim 1.02 \times 10^5$ M^{-1} (Fig. S12†). The interaction between monomer 5 and C_{60} was further observed by ^1H NMR spectroscopy when C_{60} was added into monomer 5 in $CDCl_3$ (Fig. S13†). The benzene signals shifted downfield by ~0.07 ppm. These results confirmed that monomer 5 could act as a supramolecular host with C_{60} to form **5**⊃C_{60}, suggesting that polymer **SPh** can also interact with C_{60} to form **SPh**⊃C_{60}. Mass spectrometry clearly shows the formation of the monomer **5**⊃C_{60} complex (Fig. S14†).

To understand the detailed quenching mechanisms between the photoexcited **SPh** host and C_{60} guest, we performed femtosecond transient absorption (TA) and fluorescence upconversion (FU) measurements (see ESI† for experimental details). In these experiments, the samples were pumped at 350 nm, which can excite both **SPh** and C_{60} species. Fig. 6a plots the TA spectra of **SPh** at the indicated pump–probe delays, displaying a negative feature within 400–450 nm and broadband absorptive features extending from 500 nm to the near-infrared (NIR) region. We assign the negative feature to the stimulated emission (SE) of photoexcited **SPh** and the positive features to its excited state absorption (ESA). This assignment was established by comparing the TA kinetics probed for SE and ESA to the FU kinetics measured for **SPh** (Fig. 6a). The close agreement between these three kinetic traces suggests that they all track the decay process of photoexcited **SPh**.

The TA spectra of the **SPh**⊃C_{60} complex in the presence of encapsulated C_{60} (**SPh**⊃C_{60}) are presented in Fig. 6c. In this case, the negative SE feature of **SPh** disappeared, indicating immediate depletion of the **SPh** excited state by C_{60}. This ultrafast process was further confirmed by the FU experiment. As shown in Fig. 6b, when measured under the same conditions as pure **SPh**, **SPh**⊃C_{60} displayed negligible photon counts even near time zero, suggesting that the excited **SPh** is depleted on a timescale much faster than the instrument response (≪300 fs). Based on the energy levels of **SPh** and C_{60}, we can identify this ultrafast interaction as an electron transfer from photoexcited **SPh** to C_{60}. Indeed, in the TA spectra in Fig. 6c, we observe the instantaneous formation of a positive shoulder peak at ~1080 nm that is consistent with the anion radical peak of C_{60} (C_{60}^-).[53] Meanwhile, a positive peak at ~650 nm and a broad positive band centered at ~950 nm also formed instantaneously, which can be assigned to the cation radical of **SPh** (**SPh**$^+$).[72] Clearly, C_{60}^- and **SPh**$^+$ are products of electron transfer from photoexcited **SPh** to C_{60}, and their nearly-instantaneous formation further confirmed that this electron transfer process occurred on a femtosecond timescale. This ultrafast electron transfer is likely enabled by a strong electronic coupling between **SPh** and C_{60}, which are in intimate contact due to supramolecular interactions.

The charge-separated state (**SPh**$^+$–C_{60}^-) is not very long-lived, as reflected by the decay of C_{60}^- and **SPh**$^+$ features on the ns timescale. Interestingly, accompanying this decay is the gradual formation of a positive peak at ~750 nm that coincides with the spectroscopic features of the C_{60} triplet excited state ($^3C_{60}^*$).[73] Thus, the recombination of **SPh**$^+$–C_{60}^- does not regenerate the ground state **SPh**–C_{60} but rather produces $^3C_{60}^*$. This observation is consistent with the spin–orbit charge-transfer intersystem crossing (SOCT-ISC) phenomenon that has been well documented in the literature for organic donor–acceptor systems.[74] Specifically, the orbital angular momentum change of the electron during charge recombination can induce spin-flip and populates a triplet state. A related process is also reported for semiconductor nanocrystal–organic molecule hybrid donor–acceptor systems.[75] By fitting the kinetics of **SPh**$^+$ and C_{60}^- plotted in Fig. 6d, the charge recombination (triplet formation) time was determined as ~1.1 ns. The resulting $^3C_{60}^*$ is long-lived, showing no decay within 8 ns.

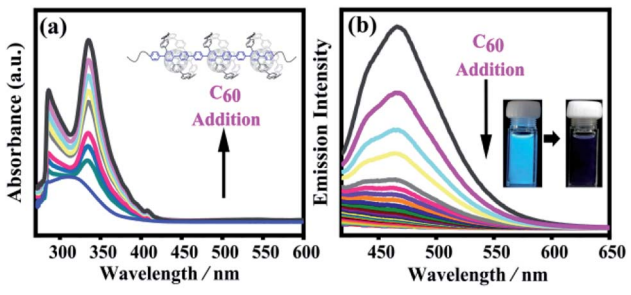

Fig. 5 (a) UV-vis absorption spectra of **SPh** (1.67×10^{-3} mg mL^{-1}) in the presence of C_{60}. (b) Fluorescence spectra of **SPh** (1.67×10^{-3} mg mL^{-1}) in the presence of C_{60}. The concentrations of C_{60} are 0.00–5.50 $\times 10^{-6}$ M. The solvent is toluene.

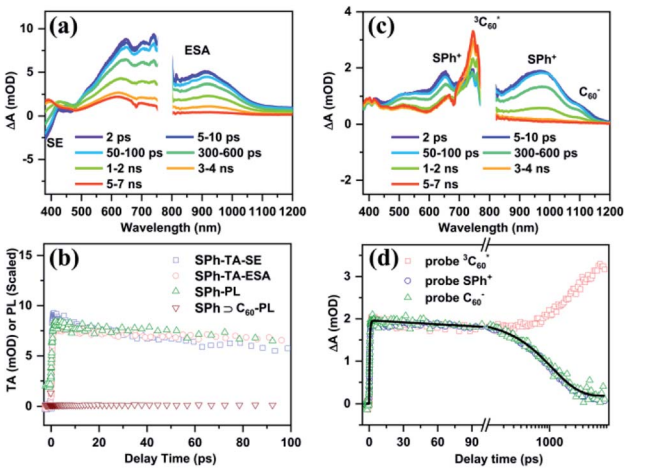

Fig. 6 TA results for **SPh**. (a) TA spectra of **SPh** probed at indicated time delays following 350 nm excitation. The SE and ESA features of **SPh** are indicated. (b) Normalized FU kinetics (green triangles) and TA kinetics of **SPh** probed at SE (blue squares) and ESA (red circles) peaks. The FU kinetics of **SPh**⊃C_{60} is also shown with wine triangles. (c) TA spectra of **SPh**⊃C_{60} probed at indicated time delays following 350 nm excitation. The absorptions of **SPh**$^+$, $^3C_{60}^*$, and C_{60}^- are also indicated. (d) Normalized TA kinetics of **SPh**⊃C_{60} probed at the $^3C_{60}^*$ (red squares), **SPh**$^+$ (blue circles), and C_{60}^- (green triangles, the black line shows the fit).

The measurements for compound **5** showed similar results to **SPh** (Fig. S15†). Thus, these time-resolved studies generally reveal femtosecond electron transfer from photoexcited compound **5** and **SPh** to encapsulated C_{60}, followed by nanosecond charge recombination to produce $^3C_{60}^*$. This offers a novel approach to sensitize $^3C_{60}^*$ that can be used to, for example, generate singlet oxygen for photocatalysis and photodynamic therapy. However, the triplet formation pathway might be detrimental to optoelectronic devices utilizing **SPh** donors and C_{60} acceptors, similar to the issue reported in organic solar cells.[76,77] Nonetheless, if the rate of charge sweeping out exceeds that of charge recombination in operating devices, triplet formation can be effectively suppressed.[78]

Charge transport properties of SPh and SPh⊃C60

Owing to the interesting photophysical properties of the polymeric structure of **SPh** and its host–guest interaction with C_{60}, we further investigated the potential applications of **SPh** and **SPh**⊃C_{60} as the electron- and hole-transport layers for optoelectronic devices.[79,80] The electron and hole mobilities (μ_e and μ_h) were measured based on the SCLC method (Fig. 7a).[81] When using only **SPh** as the electron transport layer, an electron-only device was fabricated as ITO/ZnO/**SPh**/Ca/Al. The result demonstrates that the μe value of **SPh** is ~4.87×10^{-5} cm^2 V^{-1} s^{-1} using the Mott–Gurney equation, a value which is ~2.5 times higher than that of **PS1** which we reported previously as an electron-transport layer.[44] By incorporating fullerene C_{60} into the **SPh** polymer, an electron-only ITO/ZnO/**SPh**⊃C_{60}/Ca/Al device was fabricated and the electron mobility was enhanced to ~8.06×10^{-5} cm^2 V^{-1} s^{-1}, which is higher than those of both **SPh** layer and pure C_{60} (~4.87×10^{-5} cm^2 V^{-1} s^{-1} for **SPh** and ~6.13×10^{-5} cm^2 V^{-1} s^{-1} for C_{60}).

To investigate the influence of C_{60} incorporation on the hole mobility of **SPh**, we also fabricated hole-only devices with the structure of ITO/PEDOT:PSS/active layer/MoO_3/Ag, where the active layer is **SPh**, **SPh**⊃C_{60} or C_{60}, and PEDOT:PSS is poly(3,4-ethylenedioxythiophene):poly(styrene sulfonate) (Fig. 7b) The hole mobility of **SPh** was measured to be ~2.86×10^{-5} cm^2 V^{-1} s^{-1} in the SCLC region. Interestingly, upon incorporating C_{60} into the **SPh** polymer, the hole mobility is dramatically enhanced by more than ten times to ~3.64×10^{-4} cm^2 V^{-1} s^{-1}, which is even higher than that of pure C_{60} (~9.05×10^{-5} cm^2 V^{-1} s^{-1}). Based on these results, we conclude that C_{60} incorporation enhances te charge transport properties of **SPh**, promising for applications of **SPh** and **SPh**⊃C_{60} in optoelectronic devices.

Conclusions

In conclusion, we successfully synthesized the first supramolecular polymeric heterojunction as the segment of carbon nanopeapods by incorporating the C_{60} guest into the segment of carbon nanotubes (**SPh**) containing conjugated macrocycles as the host interconnected by a PPP backbone. In the presence of C_{60}, the fluorescence intensity of **SPh** was significantly quenched. Transient absorption measurements demonstrated

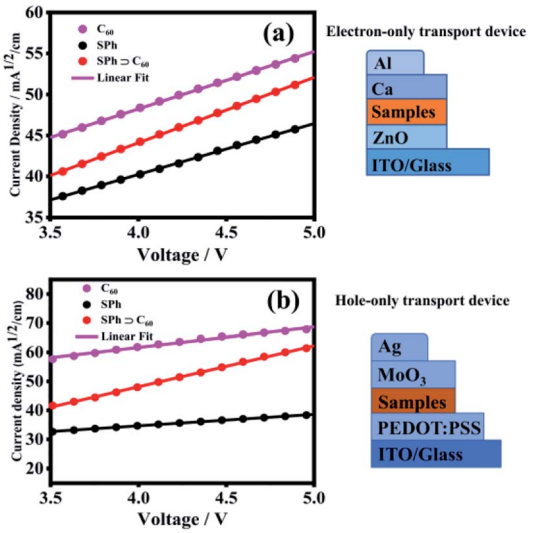

Fig. 7 $J^{1/2}$–V plots and their corresponding fitting curves of the (a) electron-only ITO/ZnO/active layer/Ca/Al device and (b) hole-only ITO/PEDOT:PSS/active layer/MoO_3/Ag device.

that, upon photoirradiation, C_{60}^- and **SPh**$^+$ are generated due to femtosecond (≪300 fs) electron transfer from the photoexcited **SPh** donor to the C_{60} acceptor, followed by nanosecond charge recombination to produce the C_{60} triplet excited state. Furthermore, compared to the host **SPh** and the guest C_{60}, the **SPh**⊃C_{60} showed enhanced electron- and hole-mobilities, promising for applications of **SPh** and **SPh**⊃C_{60} in optoelectronic devices. This study opens a door for bottom-up synthesis of carbon nanopeapod segments.

Data availability

All analytical data is provided in the ESI. All details about synthetic procedures, STM measurements, physical and photophysical characterizations are available in the ESI.

Author contributions

P. D. conceived and designed this research. S. W. synthesized the **SPh** material, conducted all characterizations and photophysical studies. J. W. and K. W. did ultrafast excited-state dynamics measurements. S. Y and X. L. performed SCLC measurements. S. W., X. L., X. Z., P. H., P. F., J. W., K. W., S. Y. and P. D. co-wrote the paper, and all the authors commented on it.

Conflicts of interest

There are no conflicts to declare.

Acknowledgements

This work was financially supported by the National Key Research and Development Program of China (2017YFA0402800), the National Natural Science Foundation of

China (21971229, 51772285, U1932214), the Fundamental Research Funds for the Central Universities and the Strategic Pilot Science and Technology Project of the Chinese Academy of Sciences (XDB17010100).

Notes and references

1 W. Zhang, W. S. Jin, T. Fukushima, A. Saeki, S. Seki and T. Aida, *Science*, 2011, **334**, 340–343.
2 B. Z. Tian, X. L. Zheng, T. J. Kempa, Y. Fang, N. F. Yu, G. H. Yu, J. L. Huang and C. M. Lieber, *Nature*, 2007, **449**, 885–889.
3 A. I. Hochbaum and P. D. Yang, *Chem. Rev.*, 2010, **110**, 527–546.
4 M. T. Björk, B. J. Ohlsson, T. Sass, A. I. Persson, C. Thelander, M. H. Magnusson, K. Deppert, L. R. Wallenberg and L. Samuelson, *Nano Lett.*, 2002, **2**, 87–89.
5 S. Banerjee and S. S. Wong, *Nano Lett.*, 2002, **2**, 195–200.
6 O. Harnack, C. Pacholski, H. Weller, A. Yasuda and J. M. Wessels, *Nano Lett.*, 2003, **3**, 1097–1101.
7 S. Günes, H. Neugebauer and N. S. Sariciftci, *Chem. Rev.*, 2007, **107**, 1324–1338.
8 K. Matsumoto, M. Fujitsuka, T. Sato, S. Onodera and O. Ito, *J. Phys. Chem. B*, 2000, **104**, 11632–11638.
9 H. Imahori, K. Hagiwara, T. Akiyama, M. Aoki, S. Taniguchi, T. Okada, M. Shirakawa and Y. Sakata, *Chem. Phys. Lett.*, 1996, **263**, 545–550.
10 T. D. M. Bell, T. A. Smith, K. P. Ghiggino, M. G. Ranasinghe, M. J. Shephard and M. N. Paddon-Row, *Chem. Phys. Lett.*, 1997, **268**, 223–228.
11 B. Grimm, H. Isla, E. M. Perez, N. Martín and D. M. Guldi, *Chem. Commun.*, 2011, **47**, 7449–7451.
12 T. Hasobe, H. Imahori, P. V. Kamat, T. K. Ahn, S. K. Kim, D. Kim, A. Fujimoto, T. Hirakawa and S. Fukuzumi, *J. Am. Chem. Soc.*, 2005, **127**, 1216–1228.
13 H. Imahori, M. Ueda, S. Kang, H. Hayashi, S. Hayashi, H. Kaji, S. Seki, A. Saeki, S. Tagawa, T. Umeyama, Y. Matano, K. Yoshida, S. Isoda, M. Shiro, N. V. Tkachenko and H. Lemmetyinen, *Chem.–Eur. J.*, 2007, **13**, 10182–10193.
14 Q. Huang, G. L. Zhuang, H. X. Jia, M. M. Qian, S. S. Cui, S. F. Yang and P. W. Du, *Angew. Chem., Int. Ed.*, 2019, **58**, 6244–6249.
15 T. Aida, E. W. Meijer and S. I. Stupp, *Science*, 2012, **335**, 813–817.
16 S. Burattini, B. W. Greenland, D. H. Merino, W. G. Weng, J. Seppala, H. M. Colquhoun, W. Hayes, M. E. Mackay, I. W. Hamley and S. J. Rowan, *J. Am. Chem. Soc.*, 2010, **132**, 12051–12058.
17 M. Burnworth, L. M. Tang, J. R. Kumpfer, A. J. Duncan, F. L. Beyer, G. L. Fiore, S. J. Rowan and C. Weder, *Nature*, 2011, **472**, 334–337.
18 T. F. A. de Greef and E. W. Meijer, *Nature*, 2008, **453**, 171–173.
19 R. J. Dong, Y. F. Zhou, X. H. Huang, X. Y. Zhu, Y. F. Lu and J. Shen, *Adv. Mater.*, 2015, **27**, 498–526.
20 J. B. Beck and S. J. Rowan, *J. Am. Chem. Soc.*, 2003, **125**, 13922–13923.
21 F. Wang, J. Q. Zhang, X. Ding, S. Y. Dong, M. Liu, B. Zheng, S. J. Li, L. Wu, Y. H. Yu, H. W. Gibson and F. H. Huang, *Angew. Chem., Int. Ed.*, 2010, **49**, 1090–1094.
22 S. Burattini, B. W. Greenland, D. H. Merino, W. G. Weng, J. Seppala, H. M. Colquhoun, W. Hayes, M. E. Mackay, I. W. Hamley and S. J. Rowan, *J. Am. Chem. Soc.*, 2010, **132**, 12051–12058.
23 S. Y. Dong, Y. Luo, X. Z. Yan, B. Zheng, X. Ding, Y. H. Yu, Z. Ma, Q. L. Zhao and F. H. Huang, *Angew. Chem., Int. Ed.*, 2011, **50**, 1905–1909.
24 B. Zheng, F. Wang, S. Y. Dong and F. H. Huang, *Chem. Soc. Rev.*, 2012, **41**, 1621–1636.
25 M. M. Zhang, X. Z. Yan, F. H. Huang, Z. B. Niu and H. W. Gibson, *Acc. Chem. Res.*, 2014, **47**, 346.
26 J. V. Barth, J. Weckesser, C. Z. Cai, P. Günter, L. Bürgi, O. Jeandupeux and K. Kern, *Angew. Chem., Int. Ed.*, 2000, **39**, 1230–1234.
27 D. C. Sherrington and K. A. Taskinen, *Chem. Soc. Rev.*, 2001, **30**, 83–93.
28 F. Würthner, Z. J. Chen, F. J. M. Hoeben, P. Osswald, C. C. You, P. Jonkheijm, J. von Herrikhuyzen, A. P. H. J. Schenning, P. P. A. M. van der Schoot, E. W. Meijer, E. H. A. Beckers, S. C. J. Meskers and R. A. J. Janssen, *J. Am. Chem. Soc.*, 2004, **126**, 10611–10618.
29 K. V. Rao, D. Miyajima, A. Nihonyanagi and T. Aida, *Nat. Chem.*, 2017, **9**, 1133–1139.
30 B. Adelizzi, P. Chidchob, N. Tanaka, B. A. G. Lamers, S. C. J. Meskers, S. Ogi, A. R. A. Palmans, S. Yamaguchi and E. W. Meijer, *J. Am. Chem. Soc.*, 2020, **142**, 16681–16689.
31 C. L. Sun, H. Q. Peng, L. Y. Niu, Y. Z. Chen, L. Z. Wu, C. H. Tung and Q. Z. Yang, *Chem. Commun.*, 2018, **54**, 1117–1120.
32 X. Zhang, L. Y. Wang, J. F. Xu, D. Y. Chen, L. Q. Shi, Y. F. Zhou and Z. H. Shen, *Gaofenzi Xuebao*, 2019, **50**, 973–987.
33 T. Aida and E. W. Meijer, *Isr. J. Chem.*, 2020, **60**, 33–47.
34 I. D. W. Samuel, G. Rumbles, C. J. Collison, R. H. Friend, S. C. Moratti and A. B. Holmes, *Synth. Met.*, 1997, **84**, 497–500.
35 D. T. McQuade, A. E. Pullen and T. M. Swager, *Chem. Rev.*, 2000, **100**, 2537–2574.
36 G. D. Scholes and G. Rumbles, *Nat. Mater.*, 2006, **5**, 920.
37 A. C. Grimsdale and K. Müllen, *Adv. Polym. Sci.*, 2006, **199**, 1–82.
38 D. L. Gin, V. P. Conticello and R. H. Grubbs, *J. Am. Chem. Soc.*, 1994, **116**, 10507–10519.
39 M. Rehahn, A. D. Schluter, G. Wegner and W. J. Feast, *Polymer*, 1989, **30**, 1054–1059.
40 Z. J. Qiu, B. A. G. Hammer and K. Müllen, *Prog. Polym. Sci.*, 2020, **100**, 101179.
41 F. N. Lu and T. Nakanishi, *Sci. Technol. Adv. Mater.*, 2015, **16**, 014805.
42 G. Grem, G. Leditzky, B. Ullrich and G. Leising, *Adv. Mater.*, 1992, **4**, 36–37.
43 K. P. Strunk, A. Abdulkarim, S. Beck, T. Marszalek, J. Bernhardt, S. Koser, W. Pisula, D. Jansch, J. Freudenberg, A. Pucci, U. H. F. Bunz, C. Melzer and

K. Müllen, *ACS Appl. Mater. Interfaces*, 2019, **11**, 19481–19488.
44 Q. Huang, G. L. Zhuang, M. M. Zhang, J. Y. Wang, S. D. Wang, Y. Y. Wu, S. F. Yang and P. W. Du, *J. Am. Chem. Soc.*, 2019, **141**, 18938–18943.
45 A. Basagni, F. Sedona, C. A. Pignedoli, M. Cattelan, L. Nicolas, M. Casarin and M. Sambi, *J. Am. Chem. Soc.*, 2015, **137**, 1802–1808.
46 R. Jasti, J. Bhattacharjee, J. B. Neaton and C. R. Bertozzi, *J. Am. Chem. Soc.*, 2008, **130**, 17646–17647.
47 C. Camacho, T. A. Niehaus, K. Itami and S. Irle, *Chem. Sci.*, 2013, **4**, 187–195.
48 K. Y. Cheung, S. J. Gui, C. F. Deng, H. F. Liang, Z. M. Xia, Z. Liu, L. F. Chi and Q. Miao, *Chem*, 2019, **5**, 838–847.
49 W. Xu, X. D. Yang, X. B. Fan, X. Wang, C. H. Tung, L. Z. Wu and H. Cong, *Angew. Chem., Int. Ed.*, 2019, **58**, 3943–3947.
50 D. Canevet, M. Gallego, H. Isla, A. de Juan, E. M. Perez and N. Martin, *J. Am. Chem. Soc.*, 2011, **133**, 3184–3190.
51 T. Iwamoto, Y. Watanabe, T. Sadahiro, T. Haino and S. Yamago, *Angew. Chem., Int. Ed.*, 2011, **50**, 8342–8344.
52 S. S. Cui, G. L. Zhuang, D. P. Lu, Q. Huang, H. X. Jia, Y. Wang, S. F. Yang and P. W. Du, *Angew. Chem., Int. Ed.*, 2018, **57**, 9330–9335.
53 Y. Z. Xu, B. Z. Wang, R. Kaur, M. B. Minameyer, M. Bothe, T. Drewello, D. M. Guldi and M. von Delius, *Angew. Chem., Int. Ed.*, 2018, **57**, 11549–11553.
54 Y. Z. Xu and M. von Delius, *Angew. Chem., Int. Ed.*, 2020, **59**, 559–573.
55 D. Canevet, E. M. Perez and N. Martín, *Angew. Chem., Int. Ed.*, 2011, **50**, 9248–9259.
56 Q. Huang, G. L. Zhuang, H. X. Jia, M. M. Qian, S. S. Cui, S. F. Yang and P. W. Du, *Angew. Chem., Int. Ed.*, 2019, **58**, 6244–6249.
57 C. Zhao, H. B. Meng, M. Z. Nie, Q. Huang, P. W. Du, C. R. Wang and T. S. Wang, *Chem. Commun.*, 2019, **55**, 11511–11514.
58 I. Khan, K. Saeed and I. Khan, *Arabian J. Chem.*, 2019, **12**, 908–931.
59 W. Zhang, M. Chen, X. D. Gong and G. W. Diao, *Carbon*, 2013, **61**, 154–163.
60 W. Zhang, X. D. Gong, C. Liu, Y. Z. Piao, Y. Sun and G. W. Diao, *J. Mater. Chem. B*, 2014, **2**, 5107–5115.
61 H. Chen, M. R. Golder, F. Wang, R. Jasti and A. K. Swan, *Carbon*, 2014, **67**, 203–213.
62 A. Abdulkarim, F. Hinkel, D. Jansch, J. Freudenberg, F. E. Golling and K. Müllen, *J. Am. Chem. Soc.*, 2016, **138**, 16208–16211.
63 E. R. Darzi, T. J. Sisto and R. Jasti, *J. Org. Chem.*, 2012, **77**, 6624–6628.
64 E. Fernandez-Bartolome, J. Santos, A. Gamonal, S. Khodabakhshi, L. J. McCormick, S. J. Teat, E. C. Sañudo, J. S. Costa and N. Martín, *Angew. Chem., Int. Ed.*, 2019, **58**, 2310–2315.
65 T. Andersson, K. Nilsson, M. Sundahl, G. Westman and O. Wennerstrom, *J. Chem. Soc., Chem. Commun.*, 1992, 604–606.
66 J. L. Atwood, G. A. Koutsantonis and C. L. Raston, *Nature*, 1994, **368**, 229–231.
67 L. Moreira, J. Calbo, R. M. K. Calderon, J. Santos, B. M. Illescas, J. Arago, J. F. Nierengarten, D. M. Guldi, E. Orti and N. Martín, *Chem. Sci.*, 2015, **6**, 4426–4432.
68 L. Moreira, B. M. Illescas and N. Martín, *J. Org. Chem.*, 2017, **82**, 3347–3358.
69 J. Xia, J. W. Bacon and R. Jasti, *Chem. Sci.*, 2012, **3**, 3018–3021.
70 T. Iwamoto, Y. Watanabe, T. Sadahiro, T. Haino and S. Yamago, *Angew. Chem., Int. Ed.*, 2011, **50**, 8342–8344.
71 Y. Z. Xu, S. Gsanger, M. B. Minameyer, I. Imaz, D. Maspoch, O. Shyshov, F. Schwer, X. Ribas, T. Drewello, B. Meyer and M. von Delius, *J. Am. Chem. Soc.*, 2019, **141**, 18500–18507.
72 E. Kayahara, T. Kouyama, T. Kato and S. Yamago, *J. Am. Chem. Soc.*, 2016, **138**, 338–344.
73 G. Sauve, N. M. Dimitrijevic and P. V. Kamat, *J. Phys. Chem.*, 1995, **99**, 1199–1203.
74 Y. Dong, A. A. Sukhanov, J. Z. Zhao, A. Elmali, X. L. Li, B. Dick, A. Karatay and V. K. Voronkova, *J. Phys. Chem. C*, 2019, **123**, 22793–22811.
75 X. Luo, Y. Y. Han, Z. W. Chen, Y. L. Li, G. J. Liang, X. Liu, T. Ding, C. M. Nie, M. Wang, F. N. Castellano and K. F. Wu, *Nat. Commun.*, 2020, **11**, 7528.
76 L. Q. Qin, X. Z. Liu, X. Zhang, J. W. Yu, L. Yang, F. G. Zhao, M. F. Huang, K. W. Wang, X. X. Wu, Y. H. Li, H. Chen, K. Wang, J. L. Xia, X. H. Lu, F. Gao, Y. P. Yi and H. Huang, *Angew. Chem., Int. Ed.*, 2020, **59**, 15043–15049.
77 A. Rao, P. C. Y. Chow, S. Gélinas, C. W. Schlenker, C.-Z. Li, H.-L. Yip, A. K.-Y. Jen, D. S. Ginger and R. H. Friend, *Nature*, 2013, **500**, 435–439.
78 Y. Q. Hou, X. Zhang, K. P. Chen, D. Y. Liu, Z. J. Wang, Q. Y. Liu, J. Z. Zhao and A. Barbon, *J. Mater. Chem. C*, 2019, **7**, 12048–12074.
79 E. Kayahara, L. S. Sun, H. Onishi, K. Suzuki, T. Fukushima, A. Sawada, H. Kaji and S. Yamago, *J. Am. Chem. Soc.*, 2017, **139**, 18480–18483.
80 A. R. Tameev, L. Y. Pereshivko and A. V. Vannikov, *Mol. Cryst. Liq. Cryst.*, 2008, **497**, 333–338.
81 P. W. M. Blom, M. J. M. deJong and J. J. M. Vleggaar, *Appl. Phys. Lett.*, 1996, **68**, 3308–3310.